



ORIGINAL ARTICLE

DOI: https://doi.org/10.4322/bds.2025.e4780

Incorporation of calcium aluminate and zirconia in polymethylmethacrylate (PMMA) bone cement for biomedical applications: study of *in vitro* osteogenesis

Incorporação do aluminato de cálcio e da zircônia no cimento ósseo de polimetilmetacrilato (PMMA) para aplicações biomédicas: estudo da osteogênese *in vitro*

Juliana dos Santos LUPP¹ ©, Luis Augusto de ALMEIDA-SILVA¹ ©, Nathalia de Souza RAMOS¹ ©, Ivone Regina de OLIVEIRA² ©, Felipe Eduardo de OLIVEIRA¹ ©, Sarah de Oliveira Marco AVELINO¹ ©, Isabela dos Santos GONÇALVES² ©, Luana Marotta Reis de VACONCELLOS¹ ©

- 1 Universidade Estadual Paulista, Instituto de Ciência e Tecnologia, Departamento de Biociências e Diagnóstico Bucal. São José dos Campos, SP, Brazil.
- 2 Universidade do Vale do Paraíba, Instituto de Pesquisa e Desenvolvimento. São José dos Campos, SP, Brazil.

How to cite: Lupp JS, de Almeida-Silva LA, Ramos NS, Oliveira IR, Oliveira FE, Avelino SOM, et al. Incorporation of calcium aluminate and zirconia in polymethylmethacrylate (PMMA) bone cement for biomedical applications: study of *in vitro* osteogenesis. Braz Dent Sci. 2025;28(4):e4780. https://doi.org/10.4322/bds.2025.e4780

ABSTRACT

Objective: To evaluate the effects of incorporating calcium aluminate cement (CAC) and monoclinic zirconia (Z) into polymethylmethacrylate (PMMA) bone cement on in vitro osteogenesis. Material and Methods: Samples of pure PMMA, PMMA+CAC 7.5% (wt%) and PMMA+Z 7.5% (wt%) were prepared. The formulations were characterized by scanning electron microscopy, energy-dispersive spectroscopy, Fourier-transform infrared spectroscopy, and wettability analysis. For biological assessment, mesenchymal stem cells derived from Wistar rat femurs were cultured on the samples. Cellular response was analyzed by cell viability assay, protein synthesis, alkaline phosphatase (ALP) activity, tumor necrosis factor-alpha (TNF-α) expression by ELISA, and mineralized nodule formation. Results: All groups exhibited cell viability greater than 70% (p>0.05). ALP activity and protein synthesis showed no significant differences (p>0.05). TNF- α expression was significantly higher in the control group (41.25 \pm 17.00 pg/mL) compared with PMMA (22.97 \pm 7.08; p<0.01), PMMA+Z (25.76 \pm 13.08; p<0.05), and PMMA+CAC (28.99 \pm 14.71; p<0.05), suggesting inflammatory modulation. All groups presented mineralized nodules. In the wettability analysis, a numerical reduction in the contact angle was observed for PMMA+Z compared with pure PMMA, but without statistical significance (p>0.05). Conclusion: The addition of CAC and Z to PMMA resulted in more homogeneous surfaces, a trend toward increased wettability, and reduced TNF- α expression, without impairing cell viability or osteogenic potential, highlighting the promising potential of these formulations for bone regeneration.

KEYWORDS

Bone cement; Calcium aluminate; Osteogenesis; Polymethyl methacrylate; Zirconia.

RESUMO

Objetivo: Avaliar os efeitos da incorporação de aluminato de cálcio (CAC) e zircônia monoclínica (Z) ao cimento ósseo de polimetilmetacrilato (PMMA) sobre a osteogênese *in vitro*. **Material e métodos:** Foram preparadas amostras de PMMA puro, PMMA+CAC 7,5% (wt%) e PMMA+Z 7,5% (wt%). As formulações foram caracterizadas por microscopia eletrônica de varredura, espectroscopia por dispersão de energia, espectroscopia no infravermelho por transformada de Fourier e análise de molhabilidade. Para avaliação biológica, células mesenquimais derivadas de fêmures de ratos *Wistar* foram cultivadas sobre as amostras. A resposta celular foi analisada por ensaio de viabilidade celular, síntese proteica, atividade de fosfatase alcalina (ALP), expressão do

fator de necrose tumoral alfa (TNF- α) por ELISA e formação de nódulos mineralizados. **Resultados:** Todos os grupos apresentaram viabilidade celular superior a 70% (p>0,05). A atividade de ALP e a síntese proteica não mostraram diferenças significativas (p>0,05). A expressão de TNF- α foi significativamente maior no grupo controle (41,25 ± 17,00 pg/mL) em comparação ao PMMA (22,97 ± 7,08; p<0,01), PMMA+Z (25,76 ± 13,08; p<0,05) e PMMA+CAC (28,99 ± 14,71; p<0,05), sugerindo modulação inflamatória. Todos os grupos apresentaram nódulos mineralizados. Na análise de molhabilidade, observou-se redução numérica do ângulo de contato para PMMA+Z em relação ao PMMA puro, porém sem diferença estatística (p>0,05). **Conclusão:** A adição de CAC e Z ao PMMA resultou em superfícies mais homogêneas, tendência de aumento da molhabilidade e redução de TNF- α , sem prejuízo da viabilidade celular ou do potencial osteogênico, evidenciando o potencial promissor dessas formulações para regeneração óssea.

PALAVRAS-CHAVE

Cimento ósseo; Aluminato de cálcio; Osteogênese; Polimetilmetacrilato; Zircônia.

INTRODUCTION

Bone is a complex tissue with unique characteristics, including regenerative capacity and high mechanical strength. The regeneration of bone defects caused by infections, trauma, tumors, or genetic disorders remains a clinical challenge that often requires the use of materials to support the regenerative process [1]. Biomaterials have emerged as an alternative to conventional autogenous bone grafts, offering biocompatibility with native tissue and modulating the cellular microenvironment to promote the formation of new bone tissue [2].

Among biomaterials, polymethylmethacrylate (PMMA)-based bone cement stands out due to its excellent mechanical properties and broad clinical applicability, being employed in bone reconstructions, fracture consolidation, and fixation of prostheses and metallic implants [3,4]. However, PMMA presents important limitations, such as the exothermic reaction during polymerization, the release of residual toxic monomers, and the absence of bioactivity, factors that may compromise tissue regeneration [5,6]. These drawbacks have motivated the search for strategies to optimize its biological performance [7], with particular emphasis on the incorporation of inorganic ceramic particles such as zirconia, calcium aluminate cement, hydroxyapatite, and zinc oxide, which can enhance cellular activity and extracellular matrix formation [4,8,9].

Calcium aluminate cement (CAC) shows great potential as a biomaterial for repairing bone defects, as its chemical composition and coefficient of thermal expansion are similar to those of human bone and teeth. CAC-based biomaterials have gained interest owing to their biocompatibility and favorable physical

and mechanical properties [10,11]. The unique microstructure and rapid setting time of this cement make it a promising candidate for bone substitution [12]. Its main advantages include reduced setting time, lower exothermic reaction, and greater mechanical strength compared with other biomaterials. The high viscosity of CAC also allows for direct and precise application at the site of the defect, reinforcing its potential for clinical use [13]. Furthermore, CAC exhibits bioactivity, evidenced by the formation of a biologically active apatite layer upon contact with body fluids, which supports cell adhesion, proliferation, and differentiation essential for bone regeneration [10-13].

Previous studies have already confirmed its biocompatibility [14], and when applied to bone defect repair, the material promoted adequate integration with both native bone and surrounding tissue [15]. Based on these properties, CAC demonstrates potential not only as a standalone biomaterial but also as an additive in PMMA cement formulations, where it contributes to significant improvements in mechanical performance, biological behavior, and dimensional stability [16].

Zirconia is a ceramic widely used in biomedical applications, regarded as one of the most durable dental ceramics, and recognized for its excellent mechanical properties, high strength, surface hardness, thermal stability, and biocompatibility [17]. Whether in its monolithic form or as a filler particle, its incorporation into biomaterials significantly contributes to structural reinforcement, enhancing resistance to wear, flexion, and fracture [18]. *In vitro* studies have demonstrated satisfactory cell viability, with low rates of corrosion, toxicity, and bacterial adhesion, underscoring its potential as a promising component in composites for bone substitution and tissue engineering applications [19,20].

Zirconia-based composites have shown encouraging biological outcomes, including greater susceptibility to new bone formation [21]. These findings strengthen the growing interest in biomaterials incorporating zirconia for hard tissue reconstruction. In this context, previous studies have demonstrated that the addition of zirconia particles to PMMA led to significant improvements in its mechanical, chemical, and biological properties, thereby expanding its clinical potential [22,23].

Taken together, the incorporation of ceramic additives such as CAC and zirconia into PMMA cement emerges as a promising strategy to overcome its biological limitations, combining adequate mechanical performance with biological properties more favorable to cellular interaction. Therefore, the present study aimed to evaluate the effects of adding CAC and zirconia to PMMA bone cement on in vitro osteogenesis, with the goal of contributing to the development of more effective composites for bone regeneration. We hypothesized that modifying PMMA cement with these ceramic additives would enhance the cellular response, promoting greater viability and osteogenic differentiation compared with pure PMMA.

MATERIAL AND METHODS

Preparation of samples

Samples of commercial PMMA cement (Biomechanics, Jaú, Brazil) were prepared according to the manufacturer's instructions. The liquid monomer was poured over the polymeric powder, and the mixture was spatulated until a homogeneous consistency was achieved. The paste was then placed into silicone molds in the shape of discs (6 mm in diameter \times 2 mm in height), yielding the pure PMMA samples.

For the PMMA + CAC group, calcium aluminate cement powder (Secar® 71, Kerneos, France), composed of the CA (CaAl $_2$ O $_4$) and CA $_2$ (CaAl $_4$ O $_7$) phases, was used. The powder was previously mixed with a polyglycol-based dispersant (0.6 wt%, BASF, Germany) and a plasticizer CaCl $_2$ ·2H $_2$ O (2.8 wt%, Labsynth, Brazil) in a dry ball mill for one hour, resulting in a homogeneous material, as described in previous studies from our research group [8,24]. The dispersant was employed to reduce particle agglomeration, favoring dispersion

and homogeneity and consequently improving system fluidity. The plasticizer was added to optimize handling and to act as a hydration accelerator, contributing to the consistency and reproducibility of the cement, as reported in the literature [14,25].

A concentration of 7.5% (wt%) of CAC was used, selected based on previous studies [26]. The CAC was then incorporated into the PMMA powder and processed again in a ball mill for one hour. The monomer was then added to the powders, followed by spatulation and molding into silicone discs (6 mm \times 2 mm). Secar® 71 has a surface area ranging from 3,700 to 4,500 cm²/g, with more than 95% of the material passing through a 90 μ m sieve [27]. This same CAC has already had its mean particle size (D₅₀) previously characterized by our group and collaborators, showing values between 8–13 μ m [15,28,29].

For the PMMA + Z group, monoclinic zirconia powder (CC10, Saint-Gobain ZirPro, France) was used. The concentration of 7.5% (wt%) was defined based on previous studies [22,23]. Zirconia powder was mixed with PMMA powder in a ball mill for one hour, followed by the addition of the monomer, spatulation, and molding into silicone discs (6 mm \times 2 mm). According to the manufacturer, CC10 zirconia has a dendritic morphology, with a mean particle size (D₅₀) of 4.5 μ m and a specific surface area ranging from 1.3 to 4.3 m²/g [30].

After molding, all samples were subjected to initial curing for 24 h at 37 °C in an oven (MA033, Marconi) under a saturated humidity atmosphere (~100% RH). Subsequently, they were demolded and stored for an additional 24 h at 37 °C. Specific molds were used for each experimental group in order to avoid cross-contamination and incorporation of residues. This methodology has already been applied in previous studies by our research group and collaborators [12,15].

Characterization of the samples

Surface topographic analysis of the samples

For this analysis, the scanning electron microscope (SEM) (JEOL/JSM-5310, Tokyo, Japan) with a Field Emission Gun (FEG) (Tescan/Vega 3, Brno, Czech Republic) was employed. The material samples were placed on an aluminum platform (stub) using a double-sided carbon tape (3M, Sumaré SP, Brazil) and were metallized with

a thin layer of gold (80 Å). This gold layer was applied through ion vaporization (sputtering) using the metalizing machine (Emitech SC 7620, Sputter Coater, Quorum Technologies, Newhaven, United Kingdom) for 130 seconds at a current of 10-15 milliamperes (mA), in a vacuum of 130 mTorr and a metallization rate of 3.5 nm/min. Images were captured using a Scanning Electron Microscope with Secondary Electron (SE) detector, which were projected onto the sample's surface.

Wetting analysis using the contact angle technique

For the wetting analysis, three samples from each group were prepared (n = 3). The average contact angle was measured using a goniometer (Ramé-Hart Inc., model 100-00-115, Mountain Lakes, New Jersey, USA) employing the sessile drop technique with distilled water as the testing liquid. Prior to analysis, each sample was carefully handled with gloves to prevent contamination. A droplet of fixed volume (5 μ L) was deposited using a gastight glass syringe (Hamilton®, model 100-10-12-22, $10 \,\mu\text{L}$ capacity, 22-gauge needle) equipped with a hydrophobic tip, allowing controlled dispensing. Measurements were performed under controlled environmental conditions (23 \pm 2 °C; relative humidity 45–55%). The contact angles on the left and right sides of each droplet were automatically calculated using DROPimage Advanced software, which also provided the final mean value for each drop.

Qualitative Analysis of the Chemical Composition of Samples by Energy Dispersive Spectroscopy (EDS)

An energy-dispersive spectrometer (Bruker Nano GmbH 410, Berlin, Germany) associated with Espirit 1.9 software (Bruker, Berlin, Germany) was utilized in conjunction with the SEM (Inspect S50, FEI Company, Brno, Czech Republic) for the qualitative analysis of chemical composition.

Fourier Transform Infrared Spectroscopy (FT-IR)

The chemical composition of the particle surfaces was analyzed using the Fourier Transform Infrared Spectrometer (Perkin Elmer, Spectrum GX model) in the UATR mode, in the midregion of 500-4000 cm $^-$ -1, with 32 scans and a resolution of 4 cm $^-$ -1, employing the Spectrom Saurch Plus program.

Cell culture

The present study was approved by the Institutional Animal Care and Use Committee (CEUA) under protocol number 02/2022, in accordance with the Ethical Principles for Animal Experimentation established by the National Council for the Control of Animal Experimentation (CONCEA).

All in vitro biological procedures were developed and executed at the Laboratory of Interdisciplinary Cell Studies. Nine rats, 90 days old and weighing approximately 300g, were euthanized by intramuscular overdose of anesthetic using an intramuscular solution of Anasedan/ Dopalen. Cells were extracted from the femurs of these rats according to Maniatopoulos et al. [31]. After femur preparation, they were placed in transport medium containing 10% Fetal Bovine Serum (FBS) (Cultilab Ltda, Campinas, Brazil) and alpha-modified with L-glutamine (α-MEM – Gibco-Life Technologies, NY, USA), and gentamicin (Gibco- Life Technologies, NY, USA). The femur ends were removed under a laminar flow hood, and osteoblast cultures were obtained from the bone marrow access of the femurs using a culture medium supplemented with essential minimal medium and 10% Fetal Bovine Serum (FBS) (Cultilab Ltda, Campinas, Brazil), alphamodified with L-glutamine (α-MEM – Gibco- Life Technologies, NY, USA), and gentamicin (Gibco-Life Technologies, NY, USA). After this procedure, the cells were placed in cell culture bottles (Kasvi, São Jose dos Pinhais, Paraná, Brazil) and stored in the incubator at 37°C with 5% CO, (Ultrasafe HF 212 UV Incubator). The nutrient supplement for the cells was changed every 72 hours, and cell culture development was evaluated through microscopy (Carl Zeiss Microscope – Axiovert 40C, Germany).

After the cells reached confluence at approximately 7 days, they were detached using a solution containing 0.25% trypsin (Cultilab Ltda, Campinas, Brazil) and counted (Cell Counter Countess®, Invitrogen, USA) to perform the viable cell plating in the wells of a 96-well plate (Kasvi, São Jose dos Pinhais, Paraná, Brazil). Prior to plating, samples of PMMA cement, PMMA + CAC, and PMMA + Z were pre-disinfected under ultraviolet (UV) light in a laminar flow hood (Bio Seg 09 Veco, Campinas, Brazil) for 30 minutes on each side and then placed within the wells of the plates.

Following this, 200 μ L of osteogenic-supplemented medium was added to the plates, which was prepared by adding 2.16g of β -glycerol phosphate (Sigma-Aldrich Chemical, St. Louis, USA) and 5 mg/mL of ascorbic acid (Neon) to a 500 mL solution of supplemented cell culture medium. The control group of the experiment was created by plating cells in the wells of the plates alone, without any sample in the well. The osteogenic-supplemented medium was changed every 72 hours.

After the completion of plating, the plates were placed in an incubator at 37°C with 5% CO2 and stored until the biological tests were conducted. The *in vitro* tests were performed in accordance with the International Organization for Standardization 10993-5 guidelines [32], and carried out in triplicate, where each triplicate consisted of a pool of cells derived from the femurs of 3 animals. The procedures for conducting the studies are detailed in previously published research by our research group Prado et al. [33], Araújo et al. [34] and Andrade et al. [35].

In Vitro biological assays

Cellular Viability Determination (MTT Assay)

After 5 days, a quantitative assessment of viable cells was conducted using the MTT dye [3-(4.5-dimethylthiazol-2-yl)-2.5diphenyltetrazolium bromide] (Sigma-Aldrich Chemical, St. Louis, USA). This solution was incubated with cells plated for four hours at 37°C in a 5% CO2 incubator, as described by Rosa et al. [36]. Following this period, the MTT solution was removed, and 200 μ l of dimethyl sulfoxide (DMSO) solution was added to the wells. The plate was agitated for 10 minutes to ensure complete solubilization. Subsequently, the 96-well plate was subjected to colorimetric measurement at a wavelength of 570 nm using a microplate reader (Biotek EL808IU). The recorded data were expressed as absorbance values and presented as a percentage.

Total protein concentration analysis

Total protein concentration was evaluated after 8 days of culture using a modified version of the method outlined by Lowry et al. [37]. After removing the culture medium, wells were washed with PBS and treated with 0.1% sodium dodecyl sulfate (SDS; Sigma-Aldrich) for protein

extraction. After 30 minutes, 1 mL of each well's solution was mixed with 1 mL of Lowry reagent (Sigma-Aldrich) and left at room temperature for 20 minutes. To this mixture, 1 mL of Folin's reagent (Sigma-Aldrich) was added for 30 minutes. After completing the reaction, absorbance was measured at 680 nm using a spectrophotometer, and the results were expressed in $\mu g/mL$. The procedures were described by Prado et al. [33] and Andrade et al. [35]

Alkaline phosphatase activity analysis

Alkaline phosphatase activity was determined after 8 days of cell plating using the same lysates used for total protein quantification. A commercial kit (LabtestDiagnóstica, Belo Horizonte, Brazil) was employed as per the manufacturer's instructions. Thymolphthalein release from thymolphthalein monophosphate substrate was measured after hydrolysis, following the methods of Prado et al. [33] and Andrade et al. [35]. A mixture of 50 μ L of thymolphthalein monophosphate and 0.5 mL of 0.3 M diethanolamine buffer at pH 10.1 was added to each well. To this mixture, 50 μ L aliquots of lysates from each well were added and incubated at 37°C for 10 minutes. To develop color, 2 mL of reagent 3 (composed of 0.09 M Na2CO3 and 0.25 M NaOH) were added. Absorbance was measured at 590 nm using a spectrophotometer (Micronal AJX 1900), and alkaline phosphatase activity was expressed as μ mol of thymolphthalein/h/ μ g of protein.

Cytokine expression measurement

At the end of the 5-day period, supernatants were collected from the wells, transferred to microtubes, and stored at -80°C. The quantification of tumor necrosis factor-alpha (TNF-α) was performed using an enzymelinked immunosorbent assay (ELISA) method. In brief, 96-well microtiter plates (Nunc) were coated with anti-TNF-α capture antibodies and incubated overnight at room temperature. The following day, plates were washed and blocked with 300 μ L of blocking buffer (1% bovine serum albumin in PBS) for 1 hour at room temperature. Subsequently, 100 µL of cell culture supernatants and cytokine or growth factor standards (TNF-α), representing the standard curve, were added to each well. Duplicate tests were conducted, and plates were incubated for 2 hours at room temperature. Following washes,

100 μL of biotin-labeled anti-TNF-α detection antibodies were added, followed by streptavidin (100 μL/well) after 2 hours. Plates were covered with aluminum foil and incubated for 20 minutes to avoid direct light. The reaction was revealed using chromogenic substrate and hydrogen peroxide. After 20 minutes, 50 μL of 2 N sulfuric acid was added to stop the reaction, and optical densities (OD) were read at 450 nm using a microplate reader (Biotek EL808IU). TNF-α levels were obtained in optical density and subsequently converted to pg/mL.

Mineralization nodule formation and calcium quantification in mineralized nodules analysis

Mineralization nodules were assessed using 2% Alizarin Red S staining (Sigma-Aldrich Chemical, St. Louis, USA) after 14 days of cell plating. Microscopic observations were carried out using a Carl Zeiss field emission scanning electron microscope (FE-SEM - EVO MA10, São Paulo, Brazil). To quantify calcium in the mineralized matrix, the method by Gregory et al. [38] was employed. Each well was treated with 10% acetic acid and incubated at room temperature with agitation for 30 minutes. The solution was transferred to centrifuge microtubes and vortexed for 30 seconds. Tubes were heated in a Dubnoff Metabolic Bath (MA095/CF) at 87.5°C for 10 minutes, followed by cooling in an ice bath and freezing for 5 minutes. After centrifugation (Labnet centrifuge - HERMLE Z 300K) for 20 minutes, $100 \,\mu\text{L}$ of the supernatant was transferred to a 96-well plate. To each well, 40 μ L of 10% ammonia hydroxide was added for acid neutralization. The absorbance was measured at 405 nm using a spectrophotometer (Micronal AJX 1900). The values were expressed as absorbance.

Cell Morphology Analysis by Field Emission Scanning Electron Microscopy (FE-SEM)

After 3 days of culture, cellular morphology was assessed using FE-SEM (Zeiss - EVO MA10, São Paulo, Brazil). Samples were washed three times with PBS to remove non-adherent cells and then chemically fixed with 4% paraformaldehyde at room temperature for 20 minutes. Subsequently, the samples were dehydrated using an ascending series of ethanol and coated with a thin layer of gold using a sputter-coating system before analysis.

Statistical analysis

The collected data were analyzed using the D'Agostino & Pearson and Shapiro-Wilk normality tests. The results confirmed the assumption of normal distribution, and the data were subjected to one-way analysis of variance (ANOVA). When significant differences were detected, Bonferroni's or Tukey's post hoc tests were applied. A significance level of 5% was adopted for all statistical tests. All analyses were performed using GraphPad Prism 7.01 software (GraphPad Inc., La Jolla, CA, USA). Each experimental group consisted of five samples (n=5) analyzed in triplicate.

RESULTS

Characterization of the samples

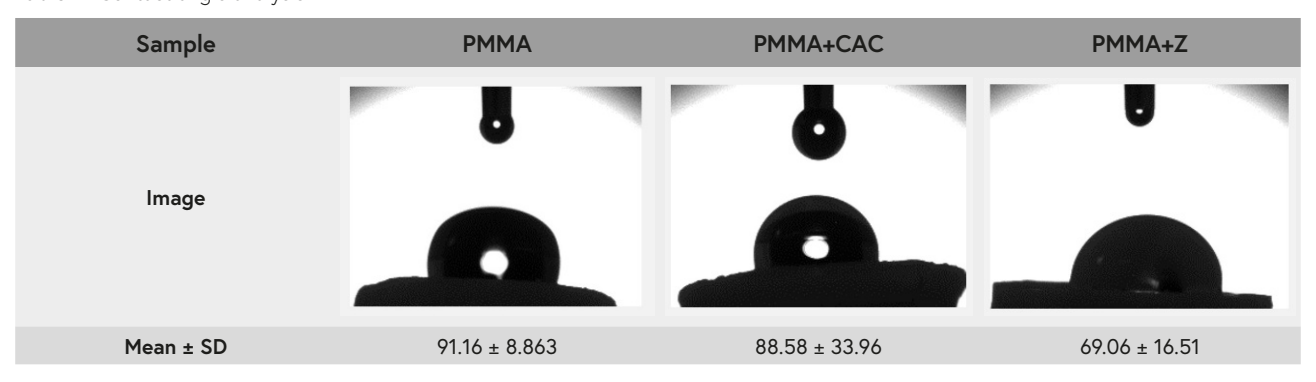
Surface topographic analysis of the samples

Surface analysis of the samples, conducted at magnifications of 500× and 2000× using SEM, was performed after 7 days of incubation. The analysis revealed significant differences in topography and morphology among the formulations of pure PMMA, PMMA with CAC (PMMA+CAC), and PMMA with zirconia (PMMA+Z) (Figure 1). In the PMMA sample (Figures 1A and 1B), the presence of larger particles and a more irregular surface topography was observed, particularly when compared to the modified formulations. These larger particles may be associated with material crystallization or insufficient homogeneous interaction among the components during synthesis. The PMMA+CAC sample (Figures 1C and 1D) exhibited a more uniform distribution of particles on the surface, indicating that the addition of calcium aluminate cement contributed to a more homogeneous interaction among the components, with a reduced presence of large particles. In the PMMA+Z sample (Figures 1E and 1F), the images revealed aggregates of smaller particles and a more homogeneous surface texture compared to pure PMMA. The incorporation of zirconia appeared to promote the formation of a more uniform matrix with improved particle dispersion.

Wetting analysis using the contact angle technique

Table I presents the mean \pm standard deviation of contact angle measurements for the PMMA, PMMA+Z, and PMMA+CAC samples.

Table I - Contact angle analysis



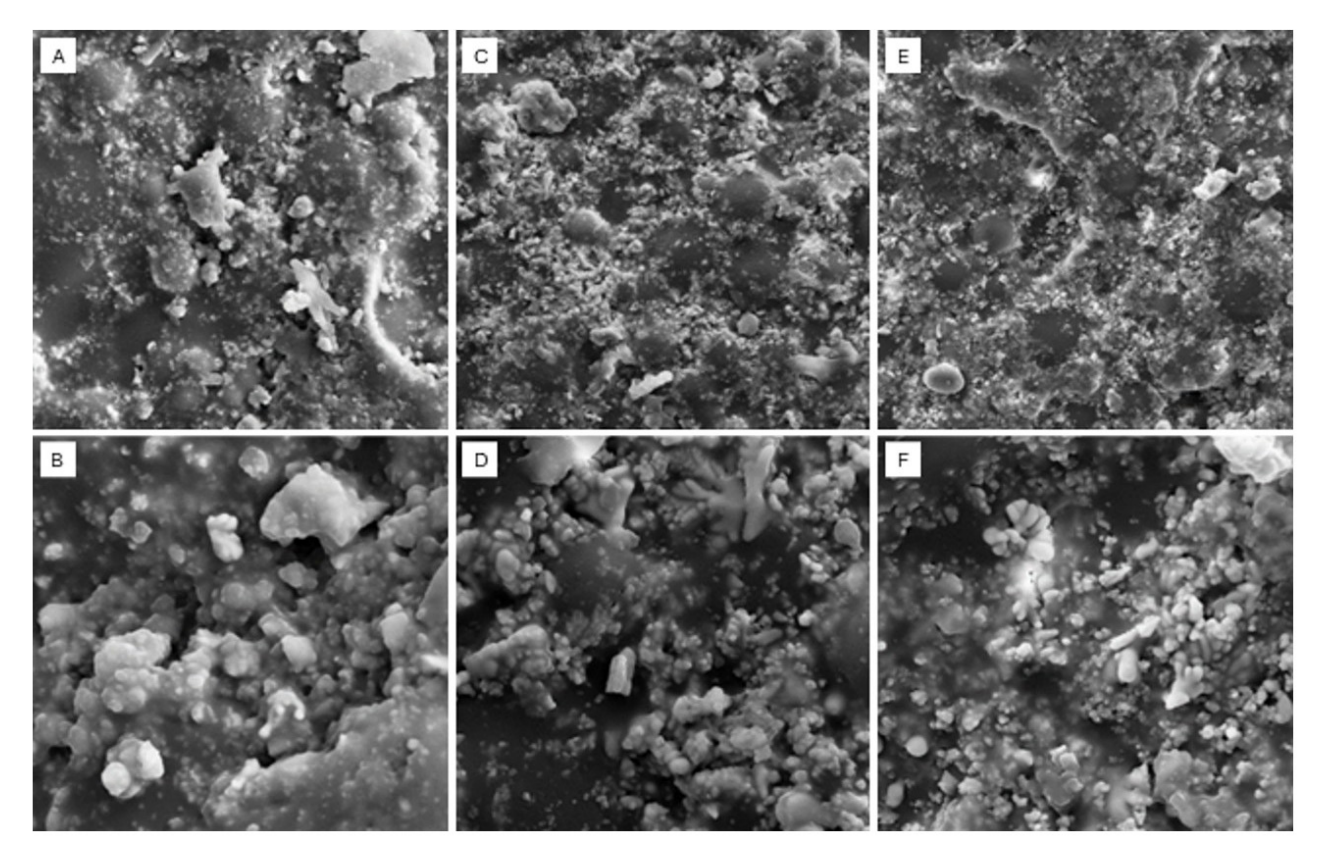


Figure 1 - Scanning electron microscopy (SEM). A) PMMA group sample of 500x; B) PMMA group sample of 2000x; C) PMMA+CAC group samples of 500x; D) PMMA+CAC group samples of 2000x; E) PMMA+Z group samples of 500x; F) PMMA+Z group samples of 2000x.

The pure PMMA sample exhibited a contact angle of 91.16 \pm 8.86°, indicating a moderately hydrophobic surface. For the PMMA+CAC sample, the contact angle was 88.58 \pm 33.96°, a value close to that of pure PMMA, suggesting that the addition of CAC did not significantly alter surface hydrophobicity. In contrast, the PMMA+Z sample showed a contact angle of 69.06 \pm 16.51°, indicating a trend toward increased surface hydrophilicity. However, statistical analysis using one-way ANOVA followed by Tukey's post hoc test revealed no significant differences between groups (p > 0.05) (Figure 2).

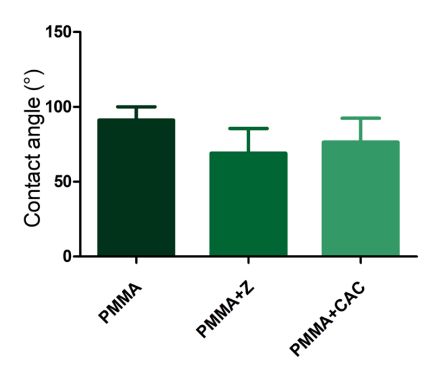


Figure 2 - Representative graph showing the mean values and standard deviation (\pm) of the wettability test (goniometry – contact angle), subjected to one-way analysis of variance (ANOVA) followed by Tukey's post hoc test.

Qualitative Analysis of the Chemical Composition of Samples by Energy Dispersive Spectroscopy (EDS)

In the EDS, a sample from each group was analyzed to ascertain the constituent chemical elements. In the samples of PMMA, when assessed through EDS, the presence of chemical elements composing the biomaterial was evidenced. Peaks of characteristic energy were primarily observed for the elements (C - Carbon, O - Oxygen; S - Sulfur, and Ba - Barium) (Figure 3). In the samples of the PMMA+CAC blend, when evaluated via EDS, the presence of

chemical elements constituting the biomaterial was highlighted. Peaks of characteristic energy were mainly observed for the elements C - Carbon, O - Oxygen; S - Sulfur, Ba - Barium; Ca - Calcium, and Al - Aluminate. In the samples of the PMMA+Z blend, when examined by EDS, the presence of chemical elements composing the biomaterial was underscored. Peaks of characteristic energy were primarily observed for the elements C - Carbon, O - Oxygen; S - Sulfur, Ba - Barium; Ca - Calcium, and Z - Zirconia. The data obtained from the measurement of chemical elements in EDS are illustrated in Table II.

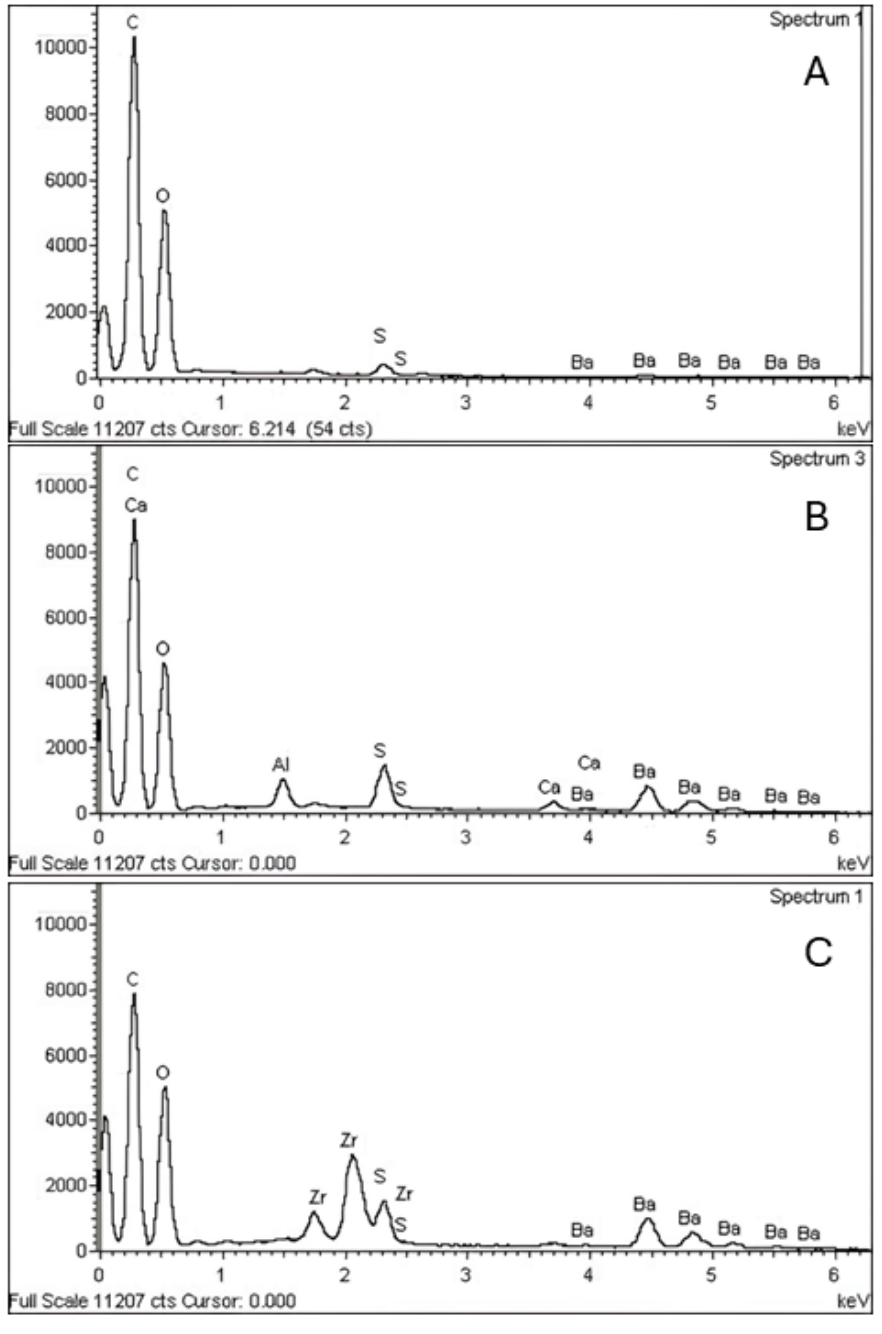


Figure 3 - Diffractogram of microanalysis by energy dispersive spectroscopy. A) PMMA; B) PMMA+CAC; C) PMMA+Z

Fourier Transform Infrared Spectroscopy (FT-IR)

Figure 4 presents the FT-IR spectra corresponding to the PMMA, PMMA+CAC, and PMMA+Z groups. The chemical composition of the samples exhibited similar bonding patterns, with no distinct evidence of additive-specific elements. The spectrum of pure PMMA displays characteristic bands associated with functional groups present in its structure, such as C=O (around 1730 cm⁻¹) and C-H (around 2950 cm⁻¹). The incorporation of calcium aluminate into PMMA may result in subtle spectral changes, such as the appearance of new bands or shifts in existing ones. These modifications are attributed to interactions between PMMA and calcium aluminate.

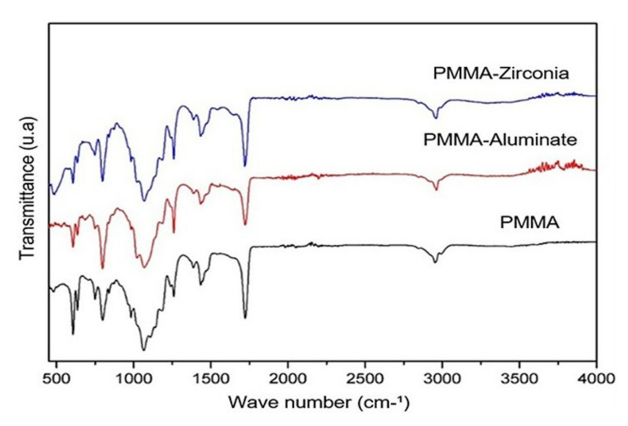


Figure 4 - Representation of bonds identified in the Fourier-transform infrared spectroscopy analysis of the particles.

Similarly, the addition of zirconia to PMMA induced alterations in the spectrum, indicating interactions between the two materials.

In Vitro biological assays

Cell morphology analysis by FE-SEM

Figure 5 presents FE-SEM micrographs of the sample surfaces from the different experimental groups: (a) PMMA, (b) PMMA+CAC, and (c) PMMA+Z, all analyzed at 1000× magnification. The images reveal the surface morphology of the biomaterials and the cellular interactions with the respective substrates after three days of cell culture. In the micrograph of the PMMA sample (Figure 5A), cells are observed adhering to the substrate; however, they exhibit a predominantly rounded morphology and are organized in clusters. Additionally, these cells display reduced cellular projections and limited elongation. In the PMMA+CAC sample (Figure 5B), there is increased cellular spreading and extension across the biomaterial surface. The cells show a more spread morphology, with elongated cellular projections. In contrast, cells on the PMMA+Z sample (Figure 5C) exhibit an intermediate morphology between those observed in the PMMA and PMMA+CAC groups. Cellular interaction appears to be less pronounced compared to the PMMA+CAC sample, with fewer projections and altered morphology.

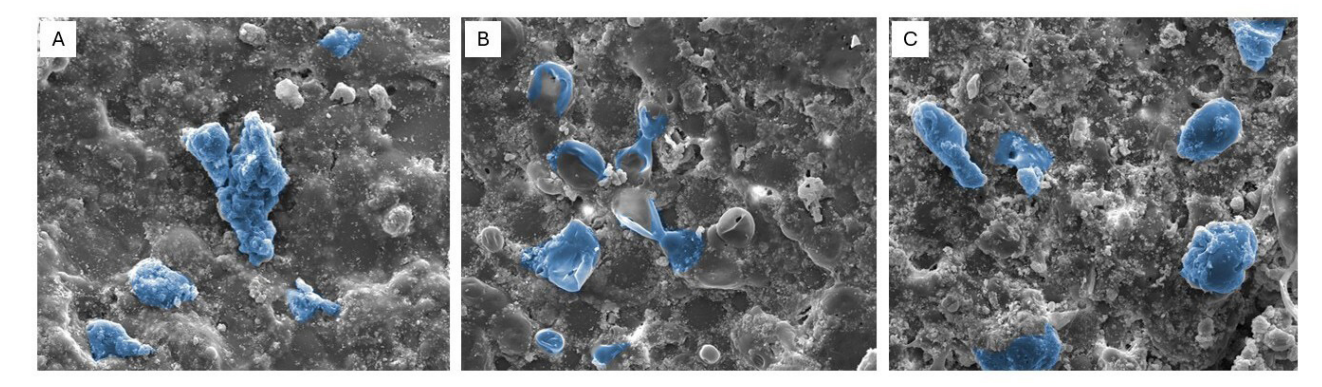


Figure 5 - Field Emission Scanning Electron Microscopy (FE-SEM) photomicrographs. A) Sample from the PMMA group at a magnification of 1000x; B) Sample from the PMMA+CAC group at a magnification of 1000x; C) Sample from the PMMA+Z group at a magnification of 1000x.

 $\textbf{Table II -} \ \textbf{Mean mass percentages (wt\%) of chemical elements detected by EDS for each sample}$

| | C (wt%) | O (wt%) | S (wt%) | Ba(wt%) | Ca(wt%) | Al(wt%) | Z (wt%) |
|----------|----------|----------|---------|---------|---------|---------|---------|
| PMMA | 51.7±0.1 | 46.5±0.4 | 0.7±0.2 | 1.2±0.4 | - | - | - |
| PMMA+CAC | 49.9±0.3 | 41.7±3.7 | 1.8±0.5 | 5.4±2.5 | 0.4±0.2 | 1.0±0.3 | - |
| PMMA+Z | 50.8±0.8 | 33.2±1.9 | 1.6±0.1 | 6.8±1.2 | - | - | 7.7±0.9 |

Wt% - Mass percentage; C - Carbon, O - Oxygen; S - Sulfur, Ba - Barium; Ca - Calcium; Al - Aluminum; Z - Zirconia.

Cellular Viability Determination (MTT Assay)

After 5 days, cellular viability data were acquired, and it was possible to ascertain that the experimental groups did not exhibit cytotoxic effects. The results underwent one-way analysis of variance (ANOVA), followed by Tukey's post hoc test, revealing no statistically significant differences among the groups (p > 0.05) (Figure 6A).

Alkaline phosphatase activity analysis

After 8 days, the alkaline phosphatase activity data were subjected to one-way analysis of variance (ANOVA), followed by Tukey's post hoc test. No statistically significant differences were observed between the groups (p > 0.05) (Figure 6B). ALP activity values were normalized to total protein content and expressed as μ mol of thymolphthalein/h/ μ g of protein to account for potential variations in cell density among the samples.

Total protein concentration analysis

After 8 days, the results of the experimental groups' total protein content were subjected

to analysis of variance (ANOVA), followed by Tukey's post hoc test. No statistically significant differences were noted among the groups (p>0.05) (Figure 6C).

Cytokine expression measurement

After 5 days, the analysis of TNF- α cytokine expression revealed a statistically significant difference between the experimental groups and the control group (p < 0.05) (Figure 6D). TNF- α concentration (pg/mL) was significantly higher in the control group (41.25 \pm 17.00) compared to the PMMA (22.97 \pm 7.08; p < 0.01), PMMA+Z (25.76 \pm 13.08; p < 0.05), and PMMA+CAC (28.99 \pm 14.71; p < 0.05) groups. No significant differences were observed among the experimental groups (p > 0.05). Statistical analysis was performed using one-way ANOVA followed by Bonferroni post hoc test.

Mineralization nodule formation and calcium quantification in mineralized nodules analysis

After 14 days of cell culture, mineralization nodules were observed in all experimental groups

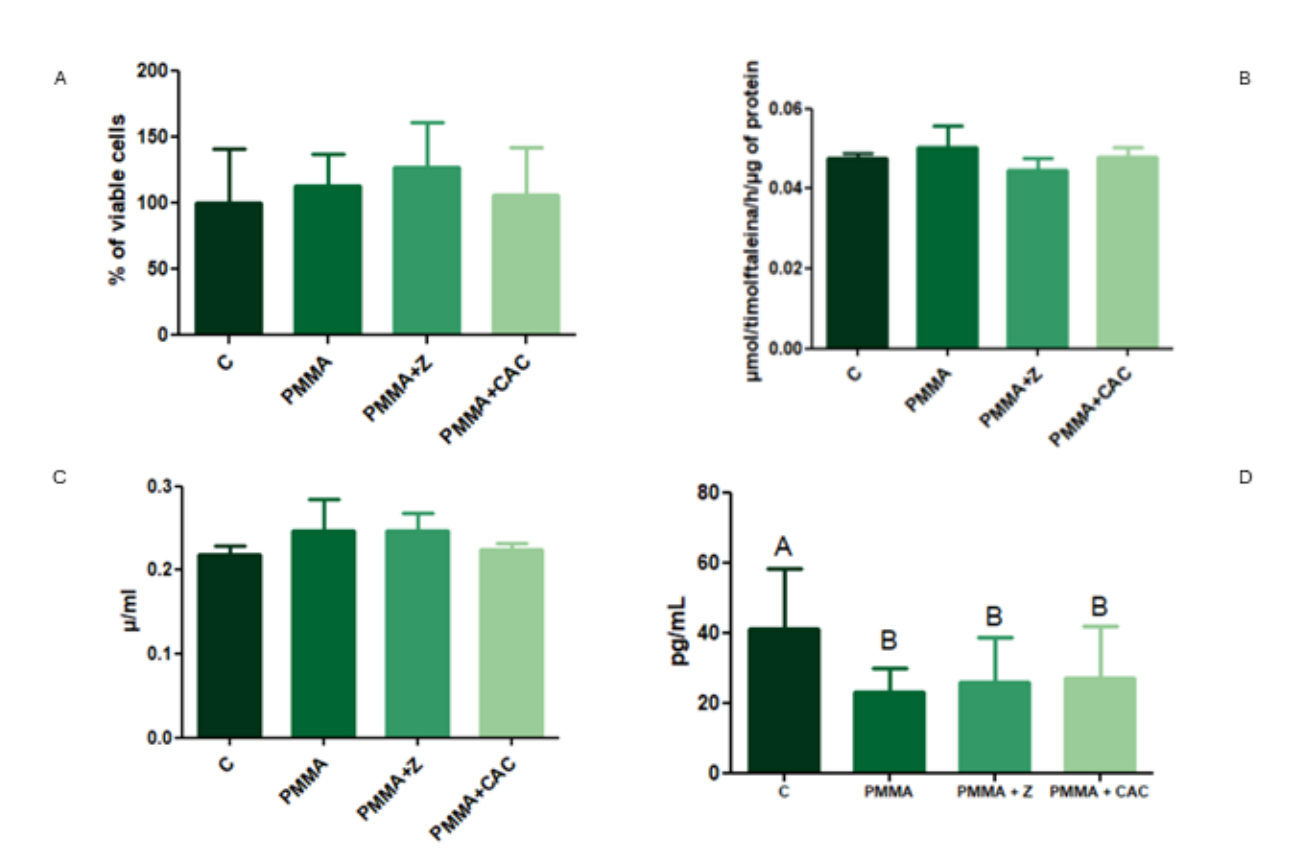


Figure 6 - Representative graphs depicting mean and standard deviation (±) values subjected to statistical analysis of variance (ANOVA), single factor. A) Cell viability test (MTT), analyzed by one-way ANOVA followed by Tukey's post hoc test; B) ALP activity test, analyzed by one-way ANOVA followed by Tukey's post hoc test; C) Total protein content test, analyzed by one-way ANOVA followed by Tukey's post hoc test; D) TNF-α cytokine expression test, analyzed by one-way ANOVA followed by Bonferroni post hoc test.

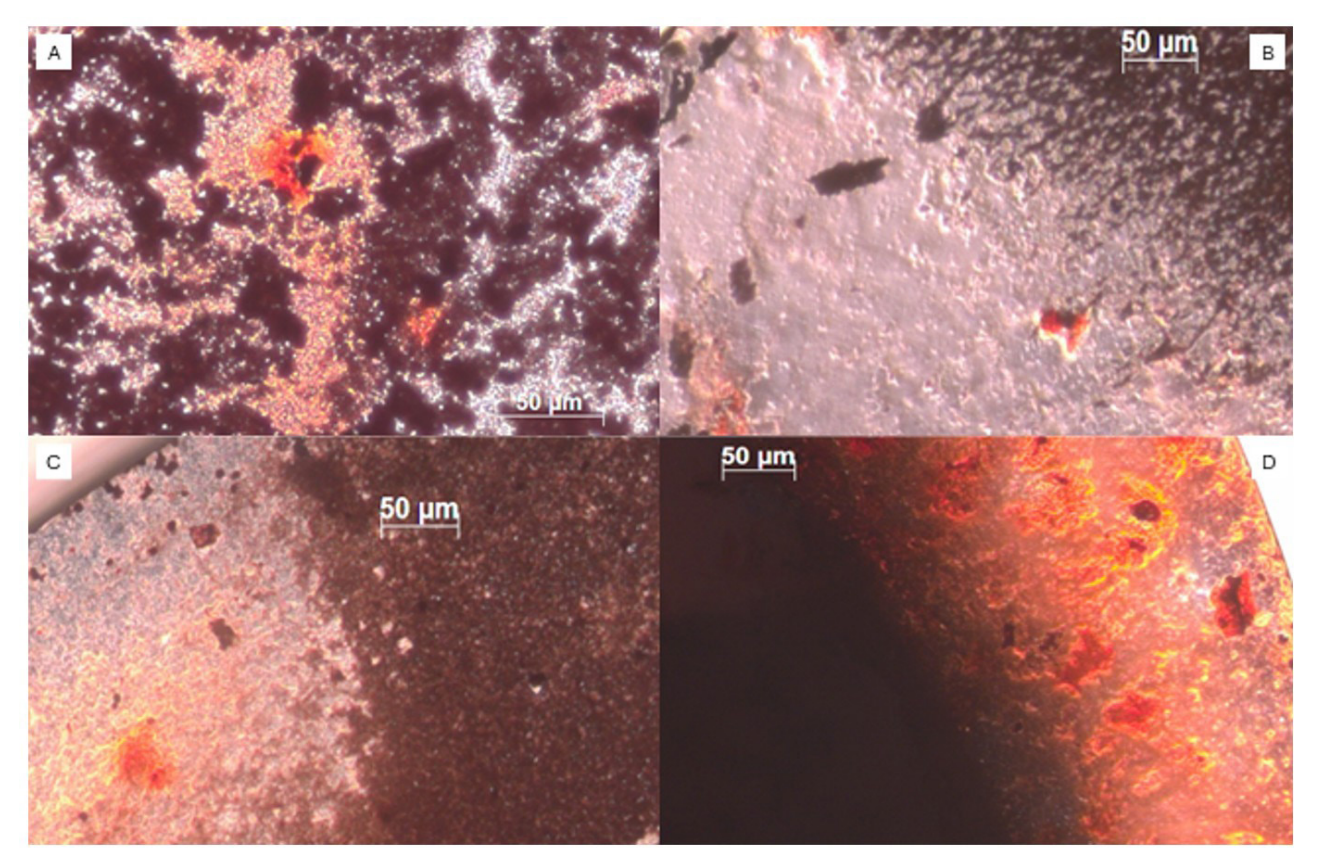


Figure 7 - Analysis of Calcium Nodule Formation in the Samples. A) Control group well under microscope magnification; B) PMMA group well under microscope magnification; C) PMMA+CAC group well under microscope magnification; and D) PMMA+Z group well under microscope magnification.

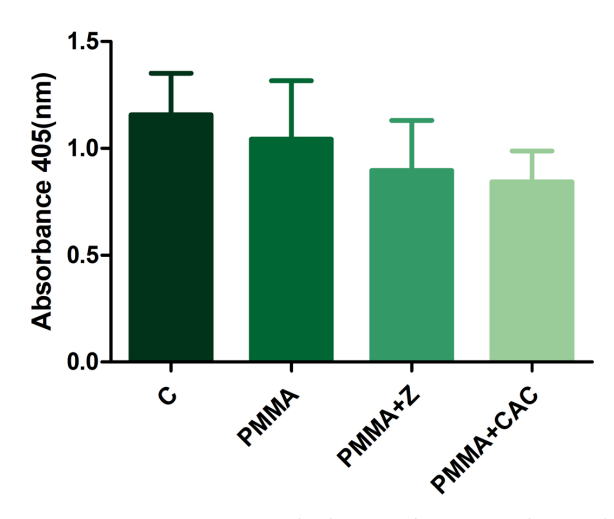


Figure 8 - Representative graph showing the mean values and standard deviation (\pm) of calcium quantification in mineralized nodules, subjected to one-way analysis of variance (ANOVA) followed by Tukey's post hoc test.

as well as in the control well. Figure 7 provides a visual representation of the nodules formed in the different experimental groups. In Figure 8, the data obtained after nodule quantification are presented. Statistical analysis was performed using one-way ANOVA followed by Tukey's post hoc test, revealing no statistically significant differences

(p > 0.05) in the amount of calcium present within the nodules among the analyzed groups.

DISCUSSION

Biomaterials can be developed from a wide range of components, including organic polymers, metals, and ceramics. The combination of these materials with other elements allows for the enhancement of their biological and mechanical properties, promoting cell proliferation and stimulating bone neoformation. Bone cements play a crucial role in prosthesis fixation by filling the space between the implant and the bone, forming a critical interface for mechanical and biological performance [39,40].

In this study, the addition of CAC and zirconia to PMMA cement was investigated with the aim of optimizing its biological and mechanical properties. Zirconia is a chemically inert ceramic with low toxicity and excellent mechanical properties, such as high flexural strength, high elastic modulus, and resistance to wear and fracture [17,41,42]. CAC, in turn, has a chemical composition and thermal expansion coefficient

similar to those of bone and dental tissue, making it a viable alternative for applications in bone regeneration and repair [12].

Although widely used in orthopedics, PMMA presents some limitations, including monomer toxicity, heat release during polymerization, excessive mechanical strength, and lack of biodegradability [5,43,44]. In our study, topographic analysis of the samples revealed that pure PMMA exhibits larger particle sizes and an irregular surface, which may compromise critical properties such as cell adhesion and structural homogeneity. These findings are consistent with the literature, which reports that pure PMMA tends to form larger particles and rougher surfaces, hindering optimal cell attachment and growth [45]. Conversely, PMMA samples modified with CAC showed a more uniform particle distribution and a more compact texture, suggesting that calcium aluminate promotes a more homogeneous interaction between components. According to studies by Parreira et al. [46], the addition of CAC to PMMA contributes to matrix compaction and porosity reduction—desirable characteristics for more durable biomaterials suited for medical applications. Similarly, the zirconia-containing formulation (PMMA+Z) presented smaller particle aggregates and a more homogeneous surface, favoring particle dispersion, which enhances both mechanical properties and cell adhesion. Previous studies have indicated that efficient dispersion of zirconia nanoparticles in the PMMA matrix results in a more uniform surface and improves the mechanical and biological performance of the composite [47,48,49].

Surface hydrophilicity was assessed by contact angle measurement, a key parameter for cell adhesion and interaction with biological fluids [50]. Pure PMMA showed a contact angle above 90°, indicating a moderately hydrophobic surface, which may limit the material's biointegration. This result corroborates previous studies that also reported high contact angles for pure PMMA, suggesting low affinity with the biological environment [51,52]. The addition of CAC did not significantly alter the material's hydrophilicity, maintaining a contact angle similar to that of pure PMMA. On the other hand, PMMA modified with zirconia showed a reduced contact angle of 69°, indicating increased hydrophilicity and, consequently, greater potential for cell adhesion. Previous studies have also shown that the incorporation of zirconia into PMMA enhances

its hydrophilic properties [53-55]. EDS analysis confirmed the presence of the expected elements in each formulation, demonstrating effective incorporation of CAC and zirconia into PMMA, with no signs of cross-contamination. FT-IR analysis indicated that the chemical structure of PMMA was preserved after the addition of the ceramic components, ensuring the structural integrity of the formulations.

SEM images revealed that pure PMMA exhibited lower cell adhesion, with dispersed cells and a rounded morphology, indicating weak interaction with the substrate. These findings are in agreement with previous studies that reported morphological alterations in cells exposed to PMMA, such as reduced elongation and altered surface morphology [56]. In contrast, PMMA samples modified with CAC showed increased cell adhesion, with more spread cells and the presence of elongated cellular projections—characteristics associated with a more favorable environment for cell attachment and proliferation, reflecting greater biocompatibility. Previous studies have reported that PMMA-CAC composites are non-cytotoxic and support cell adhesion and proliferation [57,58]. PMMA modified with zirconia demonstrated moderate cell adhesion, with cells displaying altered morphology and fewer visible projections. Although zirconia is widely used for its excellent mechanical and biological properties, Ye and Shi [59] reported that high concentrations of zirconia nanoparticles may induce cytotoxic responses in vitro, promoting morphological alterations, apoptosis, and impairing osteogenesis.

Cell viability tests, performed according to ISO 10993-5 [32] and Stoddart [60], demonstrated that none of the formulations compromised cell viability after 5 days of incubation, with values exceeding 70% and mostly comparable to the control. These results are considered satisfactory according to the aforementioned standard. Additionally, total protein synthesis and ALP expression were analyzed after 8 days of culture to evaluate cellular metabolic activity and early osteoblastic differentiation markers [61]. Although no statistically significant differences were observed between the groups, all formulations demonstrated the ability to promote protein synthesis and ALP expression, indicating that the tested composites support active cell metabolism and potential for osteogenic differentiation.

The formation of mineralization nodules, considered the final stage of osteogenic differentiation, is a complex process that, according to Hoemann et al. [62], requires extended experimental periods for accurate evaluation. After 14 days of culture, the presence of mineralized nodules was observed in all experimental groups, including the control group, confirming that cells were capable of initiating the extracellular matrix mineralization process. Despite this positive response, no statistically significant differences in calcium deposition were observed between groups. These data suggest that although the tested biomaterials did not accelerate mineralization within the analyzed timeframe, they possess osteogenic potential that may be more clearly identified in studies with longer experimental periods, encompassing more advanced stages of osteogenic differentiation [62].

TNF- α is a key cytokine in the inflammatory process, and its reduced expression indicates lower immune activation, which is beneficial for biocompatibility [63]. TNF- α analysis revealed a significant reduction in the groups containing pure PMMA, PMMA+CAC, and PMMA+Z compared to the control. Studies have shown that materials that reduce TNF- α expression are associated with better biomaterial integration and long-term tissue repair outcomes [64]. Nevertheless, it is important to consider that the presence of pro-inflammatory cytokines and a controlled degree of inflammation is necessary to initiate tissue repair [65].

CONCLUSION

The incorporation of CAC and monoclinic zirconia (CC10) into PMMA induced relevant structural modifications, resulting in more homogeneous surfaces and a trend toward decreased contact angle, increased wettability, although without statistically significant differences, as well as a significant reduction in TNF- α expression, suggesting modulation of the inflammatory response. Although all formulations exhibited adequate cell viability (>70%) and demonstrated osteogenic potential through ALP activity, protein content, and mineralized nodule formation, no statistically significant differences were observed between the groups for these osteoblastic differentiation markers. Thus, the results indicate osteogenic potential of the formulations but do not confirm an osteoinductive effect within the analyzed period. These findings highlight the

promising nature of the formulations for future applications in tissue engineering and regenerative dentistry, although further investigations are required to better elucidate their influence on osteoblastic differentiation.

Acknowledgements

The authors acknowledge the São Paulo Research Foundation (FAPESP) for the financial support granted for the execution of this study.

Author's Contributions

JSL: Conceptualization, Methodology, Software, Validation and Formal Analysis. LAAS: Writing – Original Draft Preparation, Writing – Review & Editing. NSR: Conceptualization and Methodology. IRO: Methodology and Software. FEO: Methodology and Data Curation. SOMA: Preparation, Writing – Review & Editing. ISG: Methodology and Data Curation. LMRV: Supervision, Project Administration and Funding Acquisition.

Conflict of Interest

The authors have no proprietary, financial, or other personal interest of any nature or kind in any product, service, and/or company that is presented in this article.

Funding

This study was funded by the São Paulo Research Foundation (FAPESP, São Paulo, SP, Brazil) process number 2021/09367-0.

Regulatory Statement

This study was approved by the Animal Research Ethics Committee (CEUA) under protocol number 02/2022 of the Institute of Science and Technology, São José dos Campos Campus, São Paulo State University (UNESP), in compliance with the Ethical Principles for Animal Experimentation established by the National Council for the Control of Animal Experimentation (CONCEA).

REFERENCES

 García-Gareta E, Coathup MJ, Blunn GW. Osteoinduction of bone grafting materials for bone repair and regeneration. Bone. 2015;81: 112-21. http://doi.org/10.1016/j.bone.2015.07.007. PMid:26163110.

- Thrivikraman G, Athirasala A, Twohig C, Boda SK, Bertassoni LE. Biomaterials for craniofacial bone regeneration. Dent Clin North Am. 2017;61(4):835-56. http://doi.org/10.1016/j. cden.2017.06.003. PMid:28886771.
- Lieberman IH, Togawa D, Kayanja MM. Vertebroplasty and kyphoplasty: filler materials. Spine J. 2005;5(6, Suppl):305S-16S. http://doi.org/10.1016/j.spinee.2005.02.020. PMid:16291128.
- Liu X, Cheng C, Peng X, Xiao H, Guo C, Wang X, et al. A promising material for bone repair: PMMA bone cement modified by dopamine-coated strontium-doped calcium polyphosphate particles. R Soc Open Sci. 2019;6(10):1-10. http://doi.org/10.1098/rsos.191028. PMid:31824710.
- Hamajima K, Ozawa R, Saruta J, Saita M, Kitajima H, Taleghani SR, et al. The effect of TBB, as an initiator, on the biological compatibility of PMMA/MMA bone cement. Int J Mol Sci. 2020;21(11):4016. http://doi.org/10.3390/ijms21114016. PMid:32512780.
- Alves HLR, dos Santos LA, Bergmann CP. Influência de aditivos na injetabilidade de cimento ósseo de fosfato tricálcico. Materia (Rio J). 2006;11(3):324-31. http://doi.org/10.1590/S1517-70762006000300022.
- Pahlevanzadeh F, Bakhsheshi-Rad HR, Kharaziha M, Kasiri-Asgarani M, Omidi M, Razzaghi M, et al. CNT and rGO reinforced PMMA based bone cement for fixation of load bearing implants: mechanical property and biological response. J Mech Behav Biomed Mater. 2021;116:104320. http://doi.org/10.1016/j.jmbbm.2021.104320. PMid:33571842.
- de Vasconcellos LMR, Camporês KL, de Alcântara Abdala JM, Vieira MN, de Oliveira IR. Biological and microbiological behavior of calcium aluminate cement-based blend for filling of bone defects. J Mater Sci Mater Med. 2020;31(1):10. http://doi.org/10.1007/s10856-019-6348-1. PMid:31873807.
- 9. Arora M, Chan EKS, Gupta S, Diwan AD. Polymethylmethacrylate bone cements and additives: a review of the literature. World J Orthop. 2013;4(2):67-74. http://doi.org/10.5312/wjo.v4.i2.67. PMid:23610754.
- Messias NS, Grisote G, Martorano AS, Fernandes RR, de Oliveira IR, Bombonato-Prado KF, et al. Impact of calcium aluminate cement with additives on dental pulp- derived cells. J Appl Oral Sci. 2020;28:e20190105. https://doi.org/10.1590/1678-7757-2019-0105.
- Ohtsuki C, Kamitakahara M, Miyazaki T. Bioactive ceramicbased materials with designed reactivity for bone tissue regeneration. J R Soc Interface. 2009;6(Suppl 3):S349-60. http://doi.org/10.1098/rsif.2008.0419.focus. PMid:19158015.
- de Oliveira IR, Vieira GV, Santos KW, Raniero LJ, Castro-Raucci LM, Oliveira PT, et al. Improving the radiopacity of calcium aluminate cement based blends. Mater Res. 2018;21(2):e20170599. http://doi.org/10.1590/1980-5373-mr-2017-0599.
- Burger CP, Moraes PC, Maniscalco CL, Borges PA, Batista PACS, Canola JC, et al. Cimento de aluminato de cálcio: uso em defeitos ósseos induzidos em fêmur de coelhos. Arq Bras Med Vet Zootec. 2013;65(3):757-62. http://doi.org/10.1590/ S0102-09352013000300022.
- Oliveira IR, Pandolfelli VC, Jacobovitz M. Chemical, physical and mechanical properties of a novel calcium aluminate endodontic cement. Int Endod J. 2010;43(12):1069-76. http://doi.org/10.1111/ j.1365-2591.2010.01770.x. PMid:20726916.
- Barbosa AM, dos Santos KW, Gonçalves IS, Leite PMSCM, Martorano AS, Grisote G, et al. Calcium aluminate cement blends containing bioactive glass and strontium for biomaterial applications. Mater Res. 2021;24(6):e20210223. http://doi.org/10.1590/1980-5373-mr-2021-0223.
- Jung UW, Shin JA, Chae KJ, Lee YK, Kim CK, Choi SH. The effect of LiF-maleic acid added calcium aluminate bone cement and Ca-PMMA composite bone cement on bone regeneration in rat calvarial defects. Key Eng Mater. 2007;330-332:851-4. http://doi.org/10.4028/www.scientific.net/KEM.330-332.851.

- Zhang Y, Lawn BR. Novel zirconia materials in dentistry. J Dent Res. 2018;97(2):140-7. http://doi.org/10.1177/0022034517737483. PMid:29035694.
- Gonçalves JM, Sales TAM, Figueiredo CS, Mendonça RP, Silva Júnior JP, Silva TM, et al. Multi-peak light sources can improve the physical and mechanical properties of a zirconia- and diatomite-based dental resin: an in vitro study. Braz Dent Sci. 2025;28(2):e4750. http://doi.org/10.4322/bds.2025.e4750.
- Denry I, Kelly JR. State of the art of zirconia for dental applications. Dent Mater. 2008;24(3):299-307. http://doi.org/10.1016/j. dental.2007.05.007. PMid:17659331.
- Gautam C, Joyner J, Gautam A, Rao J, Vajtai R. Zirconia based dental ceramics: structure, mechanical properties, biocompatibility and applications. Dalton Trans. 2016;45(48):19194-215. http://doi.org/10.1039/C6DT03484E. PMid:27892564.
- Bronze CSO, Grisante LAD, Araújo JCR, Guardia RS, Vicuna ILNG, Oliveira IR, et al. A new approach in bone tissue regeneration: in vivo study of the impact of calcium aluminate cement scaffolds incorporated with mesenchymal cells. Braz Dent Sci. 2025;28(1):e4296. http://doi.org/10.4322/bds.2025.e4296.
- Gad MM, Al-Thobity AM, Shahin SY, Alsaqer BT, Ali AA. Inhibitory
 effect of zirconium oxide nanoparticles on Candida albicans
 adhesion to repaired polymethyl methacrylate denture bases
 and interim removable prostheses: a new approach for denture
 stomatitis prevention. Int J Nanomedicine. 2017;12:5409-19.
 http://doi.org/10.2147/JJN.S142857. PMid:28814859.
- Gad MM, Abualsaud R, Rahoma A, Al-Thobity AM, Al-Abidi KS, Akhtar S. Effect of zirconium oxide nanoparticles addition on the optical and tensile properties of polymethyl methacrylate denture base material. Int J Nanomedicine. 2018;13:283-92. http://doi.org/10.2147/IJN.S152571. PMid:29391789.
- de Las Nieves González Vicuna I, Grancianinov KJS, dos Santos KW, dos Santos Ortega F, de Camargo Reis Mello D, de Vasconcellos LMR, et al. Scaffolds' production based on calcium aluminate blends and their biological properties. Res Biomed Eng. 2019;35(2):131-41. http://doi.org/10.1007/s42600-019-00015-0.
- Luz AP, Pandolfelli VC. Physical properties and hydration evolution of dispersant containing calcium aluminate cement compositions for endodontic applications. Ceramica. 2014;60(355):366-70. http://doi.org/10.1590/S0366-69132014000300007.
- Wang Y, Hu S, He Z. Mechanical and fracture properties of fly ash geopolymer concrete addictive with calcium aluminate cement. Materials (Basel). 2019;12(18):2982. http://doi.org/10.3390/ma12182982. PMid:31540143.
- Kerneos. Secar 71 Technical Data Sheet [Internet]. 2025 [cited 2025 Sep 7]. Available from: https://baumarket.gr/wp-content/ uploads/2018/02/Secar71.pdf
- Oliveira IR, Garcia JR, Pandolfelli VC. Cinética de hidratação de ligantes à base de alumina hidratável ou aluminato de cálcio. Ceramica. 2007;53(325):20-8. http://doi.org/10.1590/S0366-69132007000100004.
- Braulio MAL, Morbioli GG, Milanez DH, Pandolfelli VC. Calcium aluminate cement source evaluation for Al2O3–MgO refractory castables. Ceram Int. 2011;37(1):215-21. http://doi.org/10.1016/j. ceramint.2010.09.027.
- Saint-Gobain ZirPro. Monoclinic Zirconia Powders CC10. Technical Data Sheet [Internet]. 2025 [cited 2025 Sep 7]. Available from: https://www.zirpro.com/zirconia-powders/products/monoclinic-zirconia
- Maniatopoulos C, Sodek J, Melcher AH. Bone formation in vitro by stromal cells obtained from bone marrow of young adult rats. Cell Tissue Res. 1988;254(2):317-30. http://doi.org/10.1007/ BF00225804. PMid:3197089.
- ISO: International Organization for Standardization. ISO 10993-5: biological evaluation of medical devices. Part 5: tests for cytotoxicity: in vitro methods. Geneva: ISO; 2009

- Prado RF, Esteves GC, Santos ELS, Bueno DAG, Cairo CAA, Vasconcellos LGO, et al. In vitro and in vivo biological performance of porous Ti alloys prepared by powder metallurgy. PLoS One. 2018;13(5):e0196169. http://doi.org/10.1371/journal. pone.0196169. PMid:29771925.
- 34. Araújo JCR, Do Espirito Santo LL, Schneider SG, Santana Melo GF, Chaves I, Franzini DR, et al. Influence of titanium nanotubular surfaces, produced by anodization, on the behavior of osteogenic cells: in vitro evaluation,Influência da superfície nanotubular do titânio, produzido por anodização, no comportamento de células osteogênicas: avaliação in vitro. Braz Dent Sci. 2022;25(1):1-9. http://doi.org/10.4322/bds.2022.e2528.
- Andrade DP, de Vasconcellos LM, Carvalho IC, Forte LF, de Souza Santos EL, Prado RF, et al. Titanium-35niobium alloy as a potential material for biomedical implants: in vitro study. Mater Sci Eng C. 2015;56:538-44. http://doi.org/10.1016/j. msec.2015.07.026. PMid:26249625.
- Rosa AL, Crippa GE, de Oliveira PT, Taba M Jr, Lefebvre LP, Beloti MM. Human alveolar bone cell proliferation, expression of osteoblastic phenotype, and matrix mineralization on porous titanium produced by powder metallurgy. Clin Oral Implants Res. 2009;20(5):472-81. http://doi.org/10.1111/j.1600-0501.2008.01662.x. PMid:19250245.
- Lowry OH, Rosebrough NJ, Farr AL, Randall RJ. Protein measurement with the Folin phenol reagent. J Biol Chem. 1951;193(1):265-75. http://doi.org/10.1016/S0021-9258(19)52451-6. PMid:14907713.
- Gregory CA, Gunn WG, Peister A, Prockop DJ. An Alizarin red-based assay of mineralization by adherent cells in culture: comparison with cetylpyridinium chloride extraction. Anal Biochem. 2004;329(1):77-84. http://doi.org/10.1016/j. ab.2004.02.002. PMid:15136169.
- Kuhn KD. What is bone cement?. In: Breusch S, Malchau H. The well-cemented total hip arthroplasty: theory and practice, Germany: Springer; 2005. Chap. 3, p. 51-9. http://doi.org/10.1007/3-540-28924-0_5.
- Al-Rashid M, Khan W, Vemulapalli K. Principles of fracture fixation in orthopaedic trauma surgery. J Perioper Pract. 2010;20(3):113-7. http://doi.org/10.1177/175045891002000305. PMid:20642241.
- Chevalier J. What future for zirconia as a biomaterial? Biomaterials. 2006;27(4):535-43. http://doi.org/10.1016/j. biomaterials.2005.07.034. PMid:16143387.
- 42. Özcan M, Volpato CÂM, Fredel MC. Artificial aging of zirconium dioxide: an evaluation of current knowledge and clinical relevance. Curr Oral Health Rep. 2016;3(3):193-7. http://doi.org/10.1007/s40496-016-0096-9.
- Tsukimura N, Yamada M, Aita H, Hori N, Yoshino F, Chang-Il Lee M, et al. N-acetyl cysteine (NAC)-mediated detoxification and functionalization of poly(methyl methacrylate) bone cement. Biomaterials. 2009;30(20):3378-89. http://doi.org/10.1016/j. biomaterials.2009.02.043. PMid:19303139.
- 44. Xia X, Shi R, Huang J, Li Y, Zuo Y, Li J. Development of a phase change microcapsule to reduce the setting temperature of PMMA bone cement. J Appl Biomater Funct Mater. 2020;18:2280800020940279. http://doi.org/10.1177/2280800020940279. PMid:33147094.
- Henry AC, Tutt TJ, Galloway M, Davidson YY, McWhorter CS, Soper SA, et al. Surface modification of poly(methyl methacrylate) used in the fabrication of microanalytical devices. Anal Chem. 2000;72(21):5331-7. http://doi.org/10.1021/ ac000685l.
- Parreira R, Andrade T, Luz A, Pandolfelli V, Oliveira I. Calcium aluminate cement-based compositions for biomaterial applications. Ceram Int. 2016;42(10):11732-8. http://doi. org/10.1016/j.ceramint.2016.04.092.

- Motaung T, Luyt A, Saladino M, Martino D, Caponetti E, Marini V. Morphology, mechanical properties and thermal degradation kinetics of PMMA-zirconia nanocomposites prepared by melt compounding. Express Polym Lett. 2012;6(11):871-81. http://doi.org/10.3144/expresspolymlett.2012.93.
- Hu Y, Zhou S, Wu L. Surface mechanical properties of transparent poly(methyl methacrylate)/zirconia nanocomposites prepared by in situ bulk polymerization. Polymer (Guildf). 2009;50(15): 3609-16. http://doi.org/10.1016/j.polymer.2009.03.028.
- Elmadani AA, Radović I, Tomić NZ, Petrović M, Stojanović DB, Heinemann RJ, et al. Hybrid denture acrylic composites with nanozirconia and electrospun polystyrene fibers. PLoS One. 2019;14(12):e0226528. http://doi.org/10.1371/journal. pone.0226528. PMid:31851701.
- Ryszkowska JL, Auguścik M, Sheikh A, Boccaccini AR. Biodegradable polyurethane composite scaffolds containing Bioglass for bone tissue engineering. Compos Sci Technol. 2010;70(13):1894-908. http://doi.org/10.1016/j. compscitech.2010.05.011.
- Tihan T, Ioniță M, Popescu R, Iordăchescu D. Effect of hydrophilichydrophobic balance on biocompatibility of poly(methyl methacrylate) (PMMA)-hydroxyapatite (HA) composites. Mater Chem Phys. 2009;118(2-3):265-9. http://doi.org/10.1016/j. matchemphys.2009.03.019.
- Riau AK, Venkatraman SS, Dohlman CH, Mehta JS. Surface modifications of the PMMA optic of a keratoprosthesis to improve biointegration. Cornea. 2017;36(Suppl 1):S15-25. http://doi.org/10.1097/ICO.0000000000001352.PMid:28968294.
- Leão RS, Moraes SLD, Gomes JML, Lemos CAA, Casado BGDS, Vasconcelos BCDE, et al. Influence of addition of zirconia on PMMA: a systematic review. Mater Sci Eng C. 2020;106:110292. http://doi.org/10.1016/j.msec.2019.110292. PMid:31753402.
- Shahmohammadi M, Nagay B, Barão V, Sukotjo C, Jursich G, Takoudis C. Atomic layer deposition of TiO2, ZrO2 and TiO2/ ZrO2 mixed oxide nanofilms on PMMA for enhanced biomaterial functionalization. Appl Surf Sci. 2022;578:151891. http://doi. org/10.1016/j.apsusc.2021.151891.
- Riivari S, Shahramian K, Kangasniemi I, Willberg J, Närhi T. TiO2-modified zirconia surface improves epithelial cell attachment. Int J Oral Maxillofac Implants. 2019;34(2):313-9. http://doi.org/10.11607/jomi.6862. PMid:30883614.
- Katschnig M, Maroh B, Andraschek N, Schlögl S, Zefferer U, Bock E, Leitinger G, et al. Cell morphology on poly(methyl methacrylate) microstructures as function of surface energy. Int J Biomater. 2019;1:2393481. http://doi.org/10.1155/2019/2393481.
- Oliveira I, Barbosa A, Grancianinov K, Origo F, Santos K, Leite P, et al. Surface properties of calcium aluminate cement blends for bone repair applications. Ceram Int. 2020;46(9):14241-51. http://doi.org/10.1016/j.ceramint.2020.02.033.
- Oh SH, Choi SY, Choi SH, Lee YK, Kim KN. The influence of lithium fluoride on in vitro biocompatibility and bioactivity of calcium aluminate–PMMA composite cement. J Mater Sci Mater Med. 2004;15(1):25-33. http://doi.org/10.1023/ B:JMSM.0000010094.94143.a9. PMid:15338588.
- Ye M, Shi B. Zirconia nanoparticles-induced toxic effects in osteoblast-Like 3T3-E1 cells. Nanoscale Res Lett. 2018;13(1):353. http://doi.org/10.1186/s11671-018-2747-3. PMid:30402719.
- Stoddart MJ. Cell viability assays: introduction. Methods Mol Biol. 2011;740:1-6. http://doi.org/10.1007/978-1-61779-108-6_1. PMid:21468961.
- Park CS, Ha TH, Kim M, Raja N, Yun HS, Sung MJ, et al. Fast and sensitive near-infrared fluorescent probes for ALP detection and 3d printed calcium phosphate scaffold imaging in vivo. Biosens Bioelectron. 2018;105:151-8. http://doi.org/10.1016/j. bios.2018.01.018. PMid:29412939.

- 62. Hoemann CD, El-Gabalawy H, McKee MD. In vitro osteogenesis assays: influence of the primary cell source on alkaline phosphatase activity and mineralization. Pathol Biol (Paris). 2009;57(4):318-23. http://doi.org/10.1016/j.patbio.2008.06.004. PMid:18842361.
- 63. Sun J, Mu XN. Cytokine expression of cultured human endothelial cells exposed to biomaterials. Key Eng Mater. 2005;507–510:507-10. http://doi.org/10.4028/0-87849-967-9.507.
- 64. Sun H, Yang Y, Yu L, Liu K, Fei Y, Guo C, et al. Inhibition of Inflammatory response and promotion of osteogenic activity of zinc-doped microarc titanium oxide coatings. ACS Omega. 2022;7(17):14920-32. http://doi.org/10.1021/acsomega.2c00579. PMid:35557686.
- 65. Giambelluca E, Rollet-Labelle G, Bertheau-Mailhot C, Laflamme M, Pouliot M. Post-transcriptional regulation of tumour necrosis factor alpha biosynthesis: relevance to the pathophysiology of rheumatoid arthritis. Inflammation. 2013;1(1):3. http://doi.org/10.13172/2052-787X-1-1-477.

Juliana dos Santos Lupp (Corresponding address)

Universidade Estadual Paulista, Instituto de Ciência e Tecnologia, Departamento de Biociências e Diagnóstico Bucal, São José dos Campos, SP, Brazil.

Email: juliana.lupp@unesp.br

Editor: João Paulo Mendes Tribst.

Date submitted: 2025 Apr 21 Accept submission: 2025 Sep 15